



1 **Diverse Causes of Extreme Rainfall in November 2023 over Equatorial**
2 **Africa**

3

4 **Hermann N. Nana^{1*} · Masilin Gudoshava² · Roméo S. Tanessong^{3,1} · Alain T. Tamoffo⁴ ·**
5 **Derbetini A. Vondou¹**

6

7 ¹Laboratory for Environmental Modelling and Atmospheric Physics (LEMAP), Physics
8 Department, University of Yaounde 1, PO Box 812, Yaounde (Cameroon)

9

10 ²IGAD Climate Prediction and Applications Centre (ICPAC), Nairobi, (Kenya)

11

12 ³Department of Meteorology and Climatology; Higher Institute of Agriculture, Forestry,
13 Water and Environment; University of Ebolowa, PO Box 118, Ebolowa (Cameroon)

14

15 ⁴Climate Service Center Germany (GERICS), Helmholtz-Zentrum Hereon, Fischertwiete 1,
16 20095 Hamburg, Germany

17

18

19

20 * Corresponding author: Hermann N. Nana (nanahermann100@yahoo.com)

21

22 Hermann N. Nana's orcid: <https://orcid.org/0000-0002-0973-8613>

23

24 Masilin Gudoshava's orcid: <https://orcid.org/0000-0003-0315-9271>

25

26 Roméo S. Tanessong's orcid: <https://orcid.org/0000-0003-3804-5901>

27

28 Alain T. Tamoffo's orcid: <https://orcid.org/0000-0001-8482-8881>

29

30 Derbetini A. Vondou's orcid: <https://orcid.org/0000-0002-8681-5328>

31

32

33

34

35

36

37

38



39 **Abstract**

40 Understanding the atmospheric factors that lead to extreme rainfall events is
41 essential to improve climate forecasting. This study aims to diagnose the physical
42 processes underlying the extreme rainfall event of November 2023 in Equatorial Africa
43 (EA), using the ERA5 reanalysis dataset. Composite, spatio-temporal and correlation
44 analyses are used to shed light on the relationship between the November 2023 extreme
45 precipitation events and the various associated factors. The analysis reveals that these
46 extreme rainfall were mainly controlled by several factors that occurred during this period
47 in the Pacific, Atlantic and Indian oceans. These factors include strong Sea-Surface-
48 Temperature (SST) anomalies in Niño-3.4, North Tropical Atlantic, Equatorial Atlantic and
49 Indian Ocean Dipole (IOD) oceanic regions, changes in zonal winds, the Walker circulation,
50 the anomalous moisture flux and its divergence, the easterly jets and the activity of the
51 Madden-Julian Oscillation (MJO). This convergence of moisture flows entered the EA
52 region through its western and eastern boundaries, coming from the equatorial Atlantic
53 and Indian oceans respectively. The juxtaposition of these factors has led to strong and
54 positive rainfall anomalies in EA, with the highest values over the East African region,
55 mainly over southern Ethiopia, Somalia, Kenya and Tanzania, which received more than
56 430 mm of rainfall during this month. Our findings suggest that many dynamic
57 atmospheric effects need to be taken into account jointly to anticipate this type of
58 extreme event. The results of the present study contribute to the improvement of sub-
59 seasonal to seasonal rainfall forecasts by the region's national meteorological services, to
60 enable us to increase the resilience of the region's citizens to these extreme weather
61 conditions.

62 **Keywords:** Equatorial Africa, IOD, atmospheric circulation, SST, rainfall variability

63

64

65

66

67

68

69

70



71 1. Introduction

72 In recent decades, Equatorial Africa (EA) has experienced an increase in the
73 frequency and intensity of extreme events, particularly droughts, torrential rains and
74 floods (Kilavi et al. 2018). In addition, climate-sensitive sectors such as water, transport,
75 health and agriculture, among others, are negatively impacted by these events, which
76 have recently increased in magnitude and frequency. Flooding from these extreme events
77 leads to infrastructural and socio-economic damage, water shortages, severe human
78 damage and socio-economic disruption (Funk et al. 2008; Tanessong et al. 2017). With the
79 increase in greenhouse gases, the impacts of these extreme events continue and are
80 projected to increase (Gudoshava et al. 2020; Ngavom et al. 2024). East and Central
81 African countries are the regions influenced by high levels of intra-seasonal to inter-
82 annual variability in monsoon rainfall (Lüdecke et al. 2021), which are the main flood-
83 prone countries in Africa (Li et al. 2016). These exceptional flooding events generally occur
84 during October and November months, which correspond to rainy months in Central and
85 East Africa (Wainwright et al. 2020; Nicholson et al. 2022; Kenfack et al. 2024).

86 During November 2023, EA experienced a very wet period during which many
87 parts of the region were affected by extreme rainfall events, most pronounced over East
88 Africa where heavy rainfall and floods caused damage in several countries such as
89 Somalia, Ethiopia, Kenya, Burundi and Malawi ([https://floodlist.com/africa/east-africa-
90 floods-november-2023-somalia-ethiopia-kenya-burundi-malawi](https://floodlist.com/africa/east-africa-floods-november-2023-somalia-ethiopia-kenya-burundi-malawi)), causing up to 90 deaths
91 and more than 113,690 temporarily displaced. In Kenya, many areas were devastated by
92 significant flooding. At least 19 of the country's 47 counties were severely affected by the
93 floods, which started at the end of October 2023. More than 46 people lost their lives and
94 over 58,000 people have been displaced by the increased heavy precipitation and
95 subsequent flooding (<https://floodlist.com/africa/kenya-floods-update-november-2023>). In
96 Tanzania, some 10,090 people, or 2,018 households, were affected, and 1,245 houses
97 were damaged, with over 40 deaths recorded ([https://floodlist.com/africa/tanzania-floods-
98 landslides-hanang-district-december-2023](https://floodlist.com/africa/tanzania-floods-landslides-hanang-district-december-2023)). Extreme rainfall events also occurred in
99 western EA regions. Democratic Republic of the Congo (DRC), Central African Republic
100 (CAR) and Nigeria countries also experienced significant flooding and landslides which
101 affected over 90,000 people, and around ten schools and health centres were destroyed
102 ([https://www.unocha.org/publications/report/burkina-faso/west-and-central-africa-
103 weekly-humanitarian-snapshot-15-21-november-2023](https://www.unocha.org/publications/report/burkina-faso/west-and-central-africa-weekly-humanitarian-snapshot-15-21-november-2023)). These conditions have placed EA
104 in a severe food crisis. Given that climate models project a trend of increased extreme
105 rainfall in the region (Fotso-Ngeumo et al. 2019), and that the impacts of these extreme
106 events are expected to increase (Gudoshava et al. 2020), it is therefore essential to
107 understand the processes behind these extreme events.

108 Numerous studies have examined the different causes of November's extreme
109 rainfall in the EA. They have shown that these extreme events were associated with
110 numerous mechanisms linked to Sea-Surface-Temperature (SST) patterns in the tropical
111 Pacific, Atlantic and Indian Oceans (Nana et al. 2023, 2024; Palmer et al. 2023; Roy and
112 Troccoli 2024). These large-scale ocean drivers are the El Nino-Southern Oscillation (ENSO;
113 Palmer et al. 2023), Indian Ocean Dipole (IOD; Nicholson 2015; Roy and Troccoli 2024),



114 North Tropical Atlantic (NTA; [McHugh and Rogers 2001](#); [Ingeri et al. 2024](#)) and the
115 Equatorial Atlantic (ATL; [Dezfuli and Nicholson 2013](#)). [Nicholson \(2015\)](#) showed that
116 increased rainfall over East Africa is due to the presence of IOD in the October-December
117 season (OND). Following [Wahiduzzaman and Luo \(2020\)](#), several IOD episodes coincide
118 with an ENSO event, and [Zhang et al. \(2015\)](#) found that an ENSO episode can lead to the
119 development of an IOD event through the Walker circulation that connects the Indian and
120 Pacific Oceans. In this line, [Roy and Troccoli \(2024\)](#) have shown that the increase in rainfall
121 over East Africa is linked to the simultaneous presence of two factors, the IOD and ENSO.
122 [Moihamette et al. \(2022\)](#) conducted a similar study but focused on the months of
123 September-October-November over Central Africa. They found that during this period, the
124 warm (positive IOD with El Niño) and cold (negative IOD with La Niña) phases of the IOD
125 and ENSO frequently coincide. This study also showed that positive IOD events contribute
126 significantly to more rainfall in Central Africa after the El Niño effect is removed. Another
127 driver of East African rainfall is the NTA, which conducts more rainfall over many
128 countries, mainly Tanzania, Kenya and Uganda ([Ingeri et al. 2024](#)). Over western EA, the
129 Indian Ocean influences the climate system of this region through the ATL region, mainly
130 in October and November ([Moihamette et al. 2024](#)). Furthermore, in November, ENSO and
131 IOD were not considered to be important factors in many flood-affected regions,
132 particularly northern regions (north of 5° N; e.g. [Moihamette et al. 2022](#)). Consequently,
133 all the events of November 2023 were probably the result of the simultaneous occurrence
134 of several factors. These include SST in the Indian, Atlantic and Pacific oceans, the
135 atmospheric zonal circulation, Walker circulation, Madden-Julian Oscillation (MJO; [Madden
and Julian 1971, 1972](#)) activity, moisture transport and divergence and African Jets.

137 This study aims to identify and analyse the different factors that can sustain these
138 extreme rainfall events in Equatorial Africa. This paper is structured as follows: Data and
139 metrics used to diagnose mechanisms are described in [Section 2](#) and features in the EA
140 rainfall and ocean SSTs are presented in [Section 3](#). Physical processes and underlying
141 mechanisms associated with rainfall extremes are shown in [Section 4](#). [Section 5](#)
142 summarizes and concludes the document.

143 **2. Data and Methods**

144 **2.1. Data**

145 ERA5 produces monthly estimates of climate variables on a global scale, featuring
146 a horizontal resolution of 31 km (0.25° x 0.25°) and 137 vertical levels ranging from the
147 surface to 1 hPa ([Hersbach et al. 2020](#)) available from 1979 through the present. In this
148 study, we extracted ERA5 monthly data for rainfall (precip in mm day⁻¹), SST (sst in K),
149 zonal and meridional winds (u and v in m s⁻¹), specific humidity (q in Kg Kg⁻¹), vertical
150 velocity (w in m s⁻¹), surface pressure (sp in Pa), total column water vapor (tcwv in mm), 2-
151 meter dew point temperature (d2m in K), surface net solar radiation (ssr in J m⁻²) and low
152 cloud cover (lcc in %). The data span 23 vertical levels, from 1000 to 200 hPa, and cover the
153 period from November 1981 to 2023. To assess the ability of ERA5 to reproduce rainfall
154 extremes that occurred in November 2023, the observational dataset from the Climate
155 Hazards Group InfraRed Precipitation with Station dataset (CHIRPS; [Funk et al. 2015](#)) is
156 used. This dataset includes high-resolution satellite imagery and station rain-gauge data,



157 available from 1981 through the present and has a high spatial resolution of $0.05^\circ \times 0.05^\circ$.
158 The SST dataset used in this paper to analyse the oceanic conditions is provided by the
159 Extended Reconstructed Sea Surface Temperature Version 5 (ERSSTv5; [Huang et al. 2017](#)).
160 The dataset is available from 1854 through present at a resolution of $2.0^\circ \times 2.0^\circ$.

161 2.2. Methods

162 The atmospheric factors explored in this study include the DMI, zonal winds, the
163 Walker circulation over EA and the Oceans, moisture flux and divergence fields, tropical
164 SSTs in the Pacific, Atlantic and Indian Oceans, and tropical waves, namely African Easterly
165 Waves and the Madden-Julian Oscillation (MJO). We are focusing on these factors because
166 they represent the main contributors to extreme rainfall events in the EA ([Kuate et al.,
167 2019](#); [Nicholson et al. 2022](#); [Roy and Troccoli 2024](#); [Gudoshava et al., 2024](#)). The DMI is
168 calculated as the difference between SST anomalies in a western ($60^\circ \text{ E}-80^\circ \text{ E}$, $10^\circ \text{ S}-10^\circ \text{ N}$)
169 and an eastern sector ($90^\circ \text{ E}-110^\circ \text{ E}$, $10^\circ \text{ S}-0^\circ \text{ S}$) of the central Indian Ocean. Since several
170 oceans were anomalous during these extreme events, oceanic conditions of more regions
171 have been analysed. These are: the North Tropical Atlantic (NTA; $5^\circ \text{ S}-15^\circ \text{ N}$ and $40^\circ \text{ W}-15^\circ \text{ W}$),
172 the Equatorial Atlantic (ATL; $3^\circ \text{ S}-3^\circ \text{ N}$ and $20^\circ \text{ W}-10^\circ \text{ E}$) and the Niño-3.4 ($5^\circ \text{ S}-5^\circ \text{ N}$ and
173 $170^\circ \text{ W}-120^\circ \text{ W}$).

174 We start our analyses by characterizing rainfall distribution as shown by both
175 CHIRPS and ERA5 over EA (defined as $10^\circ \text{ S}-10^\circ \text{ N}$; $10^\circ \text{ E}-50^\circ \text{ E}$, see red box in [Figure 1](#)).
176 Afterwards, processes associated with November anomaly patterns are diagnosed. We
177 first look at November anomalies in SSTs and specific humidity on the one hand, and then
178 anomalies in wind and moisture flux, on the other. The zonal and meridional circulation
179 can be modulated by variations in winds and specific humidity, which can have an impact
180 on the regional hydrological cycle, either by enhancing or weakening it, following the
181 findings by [Seager et al. \(2010\)](#) and [Tamoffo et al. \(2024\)](#).

182 We have also investigated the water vapor mass transported within the zonal
183 circulation by estimating the zonal mass-weighted stream-functions (Ψ_z ; [Stachnik and
184 Schumacher 2011](#); [Taguela et al. 2022](#)), following the [Equation 1](#):

$$185 \quad \Psi_z(p) = \frac{2\pi R}{g} \int_{sp}^{P^{top}} [u] dp \quad (1)$$

186 where R is the Earth's radius (m), g is the constant of gravity, sp and P^{top} the surface and
187 top-level pressure respectively, and bracket terms denote the meridionally averaged of
188 the zonal wind over the latitudes $10^\circ \text{ S}-10^\circ \text{ N}$.

189 Note that the CB cell is characterized by the negative values of the zonal mass-
190 weighted stream-function ($\Psi_z < 0$). This function is used to characterise the Walker-type
191 circulation over the Western EA ([Longandjo and Rouault 2020](#); [Tamoffo et al. 2022](#)).
192 Environmental conditions for November 2023 are also analysed through an assessment of
193 vertically integrated moisture transport. Vertically integrated moisture flux (Q ; [Zheng and
194 Eltahir 1998](#)) is calculated using [Equation 2](#) given as follows:



195
$$Q = \frac{1}{g} \int_{sp}^{P^{top}} qV dp \quad (2)$$

196 where V is the horizontal wind (m s^{-1}).

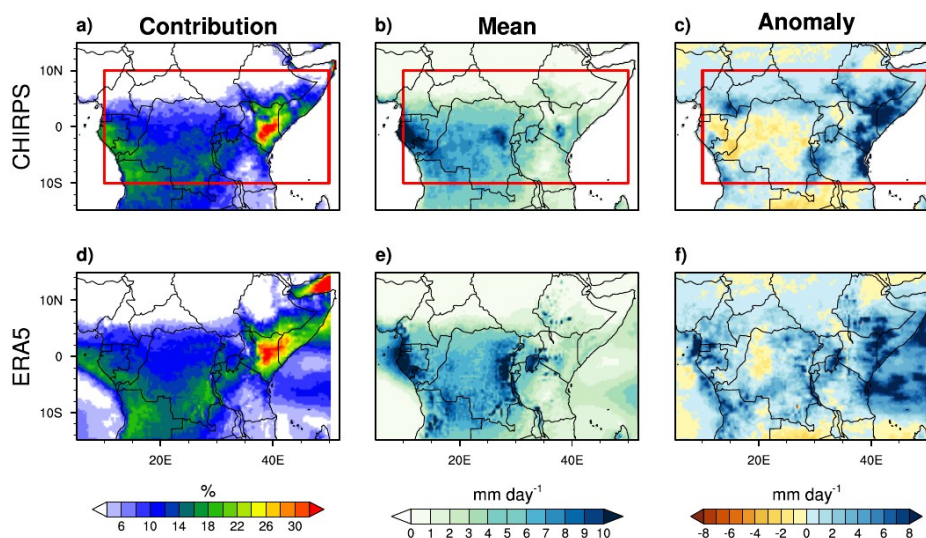
197 For all metrics used in this study, composite anomalies are obtained by removing
198 the 42-year average of the period 1981-2022. For significance testing, the student's t-test
199 is applied.

200 3. Rainfall in November 2023

201 **Figure 1** shows the percentage contribution of November rainfall to total annual
202 rainfall (**Fig. 1a,d**), November mean rainfall (**Fig. 1b,e**), and the difference between
203 November 2023 and the long-term Mean (LTM) rainfall (1981-2022; **Fig. 1c,f**). In general,
204 November 2023 was exceptionally wet throughout the EA, with more rainfall over the
205 eastern Africa area, where monthly anomalies were typically up to 7 mm day^{-1} than that
206 occurring over the western area (**Fig. 1c,f**). **Fig. 4a** features Indices of standardised rainfall
207 anomalies since 1981, based on both CHIRPS and ERA5 dataset. Extreme positive rainfall
208 anomalies occurred in 1982, 1994, 1997, 2006 and 2019 in most parts of equatorial Africa.
209 November 2023 is the strongest since 1981.

210 Positive anomalies prevail from South Sudan and Ethiopia, around 10 to 15° N , to
211 at least 10° S over the eastern region, and over northern (equator to 15° N) and southern
212 (15° S to 5° S) regions, over the western EA area in CHIRPS data (**Fig. 1c**). There is generally
213 good agreement between ERA5 and CHIRPS except in Congo Republic, northern part of
214 Gabon and central part of DRC, where ERA5 does not well estimate the negative rainfall
215 anomalies (**Fig. 1f**), and in eastern Africa regions, where ERA5 shows weaker rainfall than
216 CHIRPS. During this month, most parts of the EA region received increased rainfall of up
217 to 2 mm day^{-1} . These areas (except the northern regions) coincide with those that strongly
218 contribute to the annual EA rainfall (**Fig. 1a,d**) and normally receive at least 3 mm day^{-1} of
219 total rainfall (**Fig. 1b,e**). In the typically dry northern regions during November, rainfall
220 ranged between 3 and 9 mm day^{-1} , exceeding the long-term mean (LTM) by approximately
221 2 to 8 mm day^{-1} .

222



223
224
225
226
227

Fig 1: (a, d) Percentage contribution of November to total annual rainfall over tropical Africa, (b, e) LTM (1981-2022) rainfall for November and (c, f) November rainfall anomalies. Rainfall anomalies are calculated as the difference between CHIRPS 2023 and CHIRPS LTM rainfall.

228 4. Identifying important drivers of extreme November 2023 rainfall

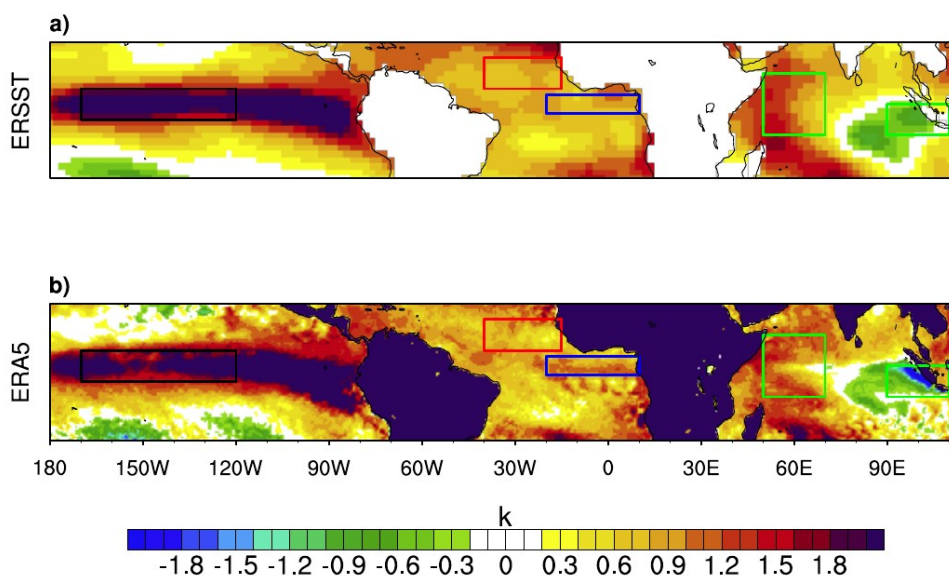
229 4.1. Sea Surface Temperatures

230

231 The tropical SST anomalies for November 2023, as estimated by ERSST and ERA5,
232 are shown in Fig. 2. In both datasets, SST anomalies were predominantly positive
233 throughout the equatorial and subtropical regions of the Pacific and Atlantic Oceans.
234 Pacific anomalies were strong and positive over the equator, where anomalies were on
235 the order of 2 to 2.9 K. That, and the positive and significant correlations with SSTs in
236 Niño-3.4 (black box in Fig. 3c) indicate that ENSO was a factor in the East African rainfall
237 anomalies of November 2023 (Chobo and Huo 2024). This ENSO observation occurs when
238 the Indian Ocean features a strong dipole pattern, with positive anomalies in the west
239 pole (10° S-10° N and 50°-70° E) and negative in the east pole (10° S-0° and 90°-110° E).
240 Many studies show that positive ENSO phases are usually associated with positive rainfall
241 anomalies over East Africa (Indeje et al. 2000; Shilenje and Ogwang 2015; Onyutha 2016).
242 However, during the two positive El Niño events, 1983 and 1992, East African countries
243 experienced significant droughts. These previous studies also found that in addition to
244 ENSO, IOD plays an important role in the modulation of precipitation in East Africa. During
245 these two years, IOD was in its negative phase. This shows that it is important to take into
246 account the combined influence of ENSO and IOD in the modulation of precipitation over
247 East Africa before and during the OND season. In this line, a recent study by Roy and
248 Troccoli (2024) showed that when IOD and ENSO are both positive in July-August-



249 September (JAS) and OND, this leads to an increased rainfall over East Africa in OND. Note
250 that in JAS 2023, these two modes were in their positive phase
251 (https://origin.cpc.ncep.noaa.gov/products/analysis_monitoring/ensostuff/ONI_v5.php;
252 <https://ds.data.jma.go.jp/tcc/tcc/products/elniyo/iodevents.html>). An important remark is
253 the similar patterns in Niño-3.4, IOD, NTA and ATL areas with those in October-November
254 2019, which were also associated with increased rainfall over East Africa (Nicholson et al.
255 2022; Ingeri et al. 2024).
256



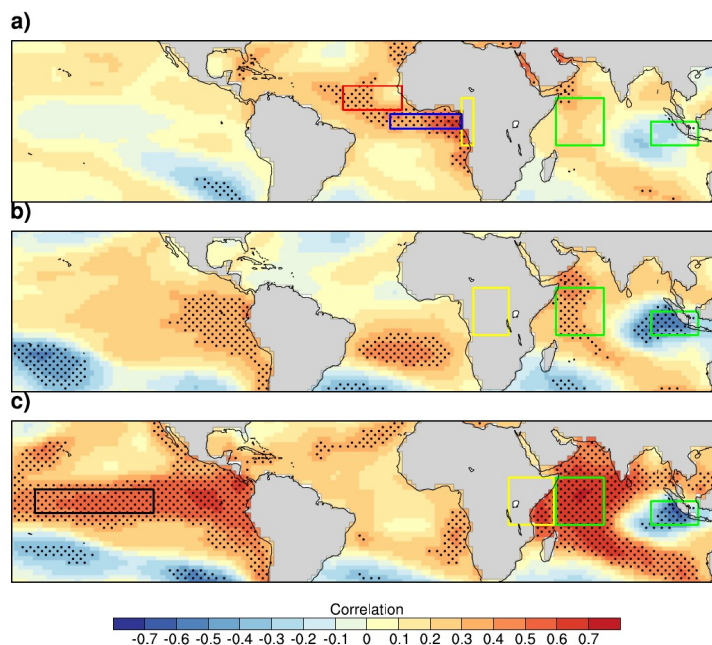
257
258 **Fig 2:** SST anomalies during November 2023 for (a) ERSST and (b) ERA5. Red and blue boxes
259 indicate the areas for north tropical Atlantic (NTA; 5°-15° N and 40°-15° W) and equatorial Atlantic
260 (ATL; 3° S-3° N and 20° W-10° E) SST calculations, green boxes indicate the areas for DMI
261 calculation. The black box over the Pacific Ocean is Niño-3.4 (5° S-5° N and 170°-120° W).
262

263 The time series of SSTs for the Niño-3.4 region over the period 1981-2023 (black
264 line in Fig. 4c) indicates the warmth in November 2023. During this period, the 2023
265 anomalies ranked among the three warmest years on record. This Pacific sector exhibits
266 the strongest correlation with November rainfall over the CB (Moihamette et al. 2022) and
267 over eastern EA (Fig. 3c; Palmer et al. 2023; Chobo and Huo 2024; Roy and Troccoli 2024).
268 These SST anomalies likely played a key role in the positive rainfall anomalies observed in
269 eastern EA, especially in coastal areas, as well as in the CB. Roy and Troccoli (2024) showed
270 that when IOD and ENSO are both positive in November, this contributes to excessive
271 rainfall over the whole of East Africa, south of the DRC, north of Angola, Nigeria and CAR,
272 while deficit rainfall occurs over certain parts of DRC. In this line, the study by Moihamette
273 et al. (2022) showed that during simultaneous both positive IOD and ENSO events, the
274 influence of the positive phase of IOD on EA rainfall is significant with the non-El Niño



275 effect and this is characterized by an increase in moisture advection toward EA that
276 contributes to an enhancement of rainfall intensity, more pronounced over eastern and
277 western EA.

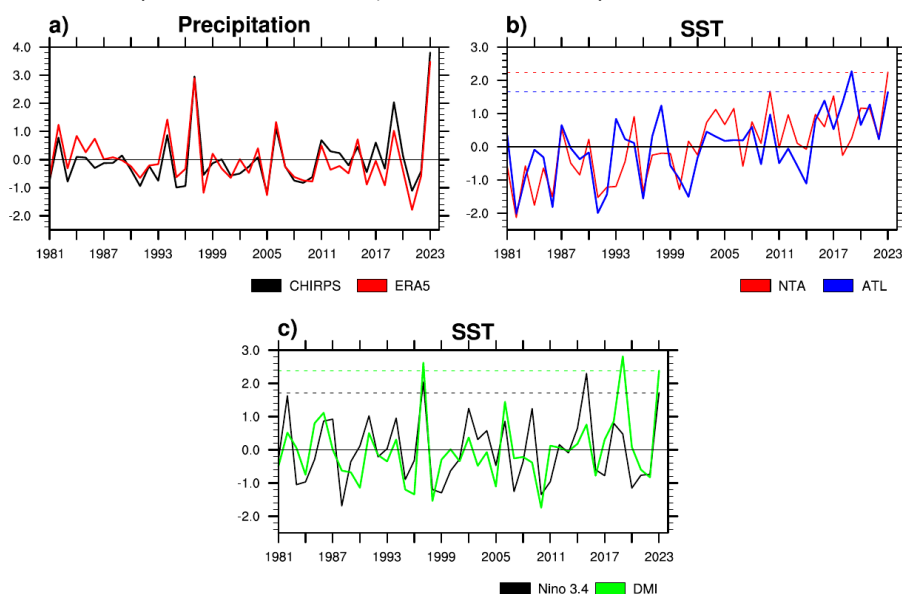
278 Extreme positive values were recorded in November 1997, 2006, and 2019, all of
279 which were exceptionally wet years in eastern EA. The 2023 positive dipole event ranks as
280 the third strongest for November since 1981. Notably, the DMI magnitude in 2023 was
281 smaller than in both November 1997 and 2019, when conditions in EA were considerably
282 drier than in 2023, suggesting that additional factors may have contributed. The event
283 may have influenced the CB, as significant correlations between the DMI and rainfall are
284 evident (Fig. 3b), with the strongest impact observed in the far eastern EA region (Dezfuli
285 and Nicholson, 2013). However, rainfall anomalies within CB exhibit both positive and
286 negative values, which can be linked to the IOD due to significant correlations over the
287 IOD regions. While heavy rainfall in both CB and eastern Africa is likely associated with the
288 IOD, this does not hold true for other affected areas. Following Dezfuli and Nicholson
289 (2013), correlations between SST and rainfall suggest that November rainfall in western EA
290 is not influenced by the IOD, a conclusion further reinforced by the correlations in Fig. 3a.
291



292
293 **Fig 3:** Correlation coefficient between (a) Western EA (10° E-15° E), (b) Congo Basin (CB;15° E-30° E),
294 and (c) Eastern EA (30° E-50° E) rainfall with SST during 1981-2023 period. The stippling occurs
295 where the correlation is statistically significant at the 95% confidence level through the Student's t
296 test
297



298 The intense rainfall in western EA can likely be attributed to the Atlantic SST
299 anomalies. It is important to highlight that SSTs along the eastern Atlantic coast and in the
300 central equatorial Atlantic show a strong positive correlation with November rainfall in
301 western EA, as reported by Lutz et al. (2014). Figure 3a shows correlations of western EA
302 November rainfall with SSTs. Over the Atlantic Ocean, significant and positive correlations
303 between western EA rainfall and SST occur over NTA, ATL and eastern Atlantic coastal
304 regions (Fig. 3a). Moihamette et al. 2024 suggest that in November, the Atlantic Ocean has
305 a significant influence during positive IOD events, induced by its teleconnection with the
306 Indian Ocean. This is characterized by anomalous westerly winds over the central
307 equatorial Atlantic Ocean (ATL, blue box in Fig. 3a), generating moisture advection
308 towards western EA. These winds originate from the NTA domain (red box in Fig. 3a).
309 Furthermore, these ocean regions feature strong standardised SST anomalies in 2023 (Fig.
310 4b). A feature to note is the exceptional warmth of SSTs in November 2023 over the NTA
311 area (red line in Fig. 4b). Over the 1981-2023 period, the 2023 anomalies were the
312 warmest on record. Another feature of NTA variability is its positive correlation ($r > 0.2$)
313 with eastern EA rainfall (Fig.3c). A recent study by Ingeri et al. (2024) showed that positive
314 SST anomalies in NTA from October to December lead to enhanced East African rainfall,
315 mainly over Tanzania, Kenya and southern Uganda. In addition, the SST time series over
316 the equatorial Atlantic showed that the 2023 anomalies were the second warmest year
317 after the November 2019 anomalies which led to a significant increase in rainfall over
318 western EA (Nicholson et al. 2022; Kenfack et al. 2024).



319
320 **Fig 4:** (a) Indices of standardised rainfall anomalies over 1981-2023, averaged over the red box
321 indicated in Fig. 1. (b) As in (a), but averaged for the SST over the NTA and ATL oceanic regions. (c)
322 As in (a), but averaged for the DMI and Niño-3.4.



323

324 **4.2. Dynamic factors associated with the November 2023 extreme rainfall**

325 Many studies (eg., Pokam et al. 2012, 2014; Taguela et al., 2022) proposed a
326 physical mechanism for modulating the long rains over CB on interannual timescales.
327 They identified that changes in the low-level westerlies (LLW) over the equatorial Atlantic
328 Ocean play a significant role in this modulation. These westerlies influence the moisture
329 transport and atmospheric conditions over the region (Nana et al. 2023), impacting the
330 onset, intensity, and duration of the long rains. Variations in LLW can alter the regional
331 climate patterns, and this mechanism helps explain the variability of the long rains in
332 relation to other climatic phenomena, such as the ENSO.

333 The maximum moisture convergence over equatorial central Africa in SON is found
334 to be a consequence of low-level moisture advection from the Atlantic Ocean. These LLWs
335 are controlled by the heating contrast between cooling associated with subsidence over
336 the ocean and heating over land regions, where ascent prevails. These heating contrasts
337 lead to a Walker-type circulation over the Atlantic Ocean and equatorial central Africa with
338 the development of LLW as its lower branch. These LLW over the equatorial Atlantic are
339 strongly correlated with DMI (Moihamette et al. 2024). For East Africa rainfall variability,
340 numerous studies have identified ENSO and IOD as the two main atmospheric drivers that
341 influenced the October-November-December (OND) rainfall (Indeje et al. 2000; Shilenje
342 and Ogwang 2015; Roy and Troccoli 2024). Following Black (2005), these drivers play an
343 important role in the moisture convergence over East Africa through moisture advection
344 from the Indian Ocean, even if they are not independent of each other. Roy and Troccoli
345 (2024) showed that when ENSO and IOD are in the same phase during JAS, The Walker-like
346 circulation appears to play a major role in modifying the ascending branch into a
347 descending branch in two situations (positive and negative phases) during OND period.

348 **4.2.1. Zonal circulation/winds, Walker circulation and water vapor mass transported** 349 **over tropical Oceans**

350

351 Following the recent study of Longandjo and Rouault (2024), rainfall variability over
352 EA is highly dependent on moisture inputs linked to atmospheric circulation. It is
353 therefore important to show the characteristics of these moisture inputs to identify their
354 oceanic origin.

355 Figure 5 depicts the vertical profile of specific humidity (first row) and zonal
356 moisture flux (shaded) overlaid by zonal wind (contour; second row) in November for the
357 climatology of 1981-2022 (Fig. 5a,d), 2023 average (Fig. 5b,e) and the anomaly (Fig. 5c,f),
358 averaged between 10° S-10° N.

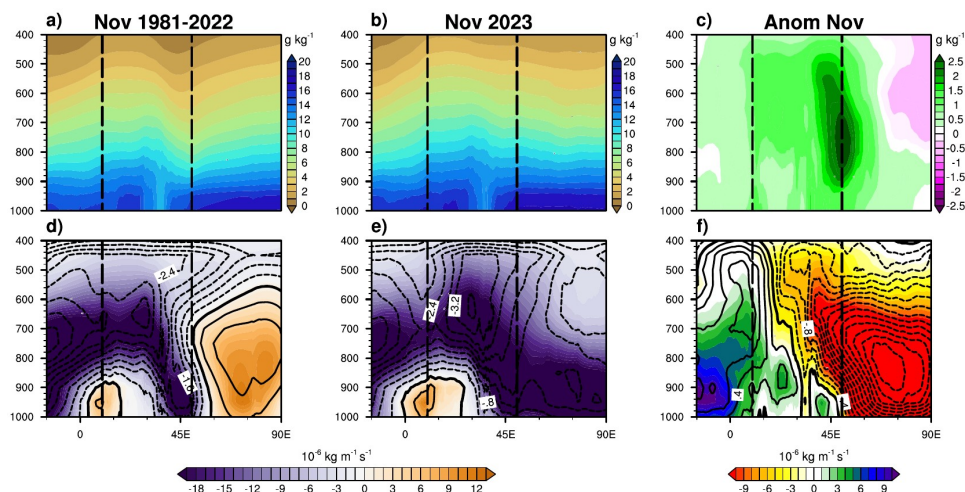
359 Over the Indian Ocean, the 1981-2022 climatology is characterized by intense
360 westerly flux, whereas the November 2023 average appears to be an easterly flux (Fig.
361 5d,e). Over the continent, moisture flux is predominantly easterly or westerly during
362 November 2023 as in the climatology. We can conclude from this that two distinct



363 mechanisms govern the moisture flux over the Indian Ocean and the continent. It is
364 noteworthy that the anomaly analysis (Fig. 5c) confirms that there was more moisture
365 over the EA in November 2023 than in the 1981-2022 climatology. This moisture surplus
366 appears here to extend up to 400 hPa and is more pronounced over eastern EA between
367 900 and 500 hPa.

368 In addition, from the Atlantic Ocean, the westerly wind in 2023 was more
369 pronounced near 30° E compared to the climatology (near 17° E). These results lead to a
370 strong moisture flux from the Atlantic (Indian) Ocean over western (eastern) EA (Fig. 5f),
371 following the work of Chadwick et al. (2016) who showed that increased humidity over
372 land would be a response to increased moisture advection from the oceans under
373 warming. The easterly flux over eastern EA is strong at the middle troposphere, where
374 strong moisture is observed. It is interesting to note that the intensity of the LLW
375 anomalies appears to extend to the upper troposphere. In conclusion, the intensification
376 of the zonal wind over EA indicates that this moisture (strong from 900 hPa) probably
377 comes from both the equatorial Atlantic and Indian Oceans.

378



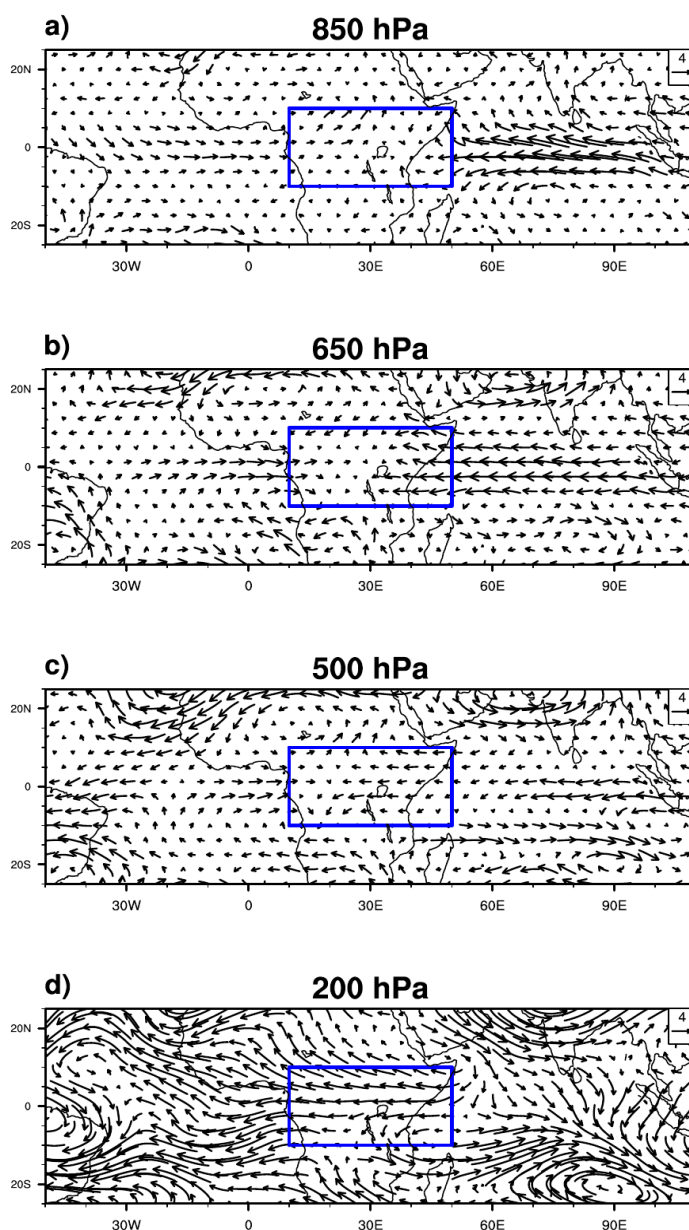
379
380 **Fig 5:** Longitude-height cross-sections of (first row) specific humidity and (second row) zonal
381 moisture flux (shaded: 10⁻⁶ kg m⁻¹ s⁻¹) and zonal wind (contour: m s⁻¹) for (a,d) the climatology of
382 November 1981-2022, (b,e) November 2023 and (c,f) the anomaly, averaged between 10° S-10° N.

383

384 The precedent anomaly analysis leads us to conclude that both the Atlantic and
385 Indian oceans contribute to the moisture increase (so more rainfall in November 2023)
386 over the EA and that ENSO has a possible contribution mainly over the eastern EA. This
387 suggests large-scale tropical climate control. To examine the links with tropical circulation,
388 large-scale wind, omega and water vapor mass transported field analyses are carried out,
389 and the results are present in Figures 6-9.



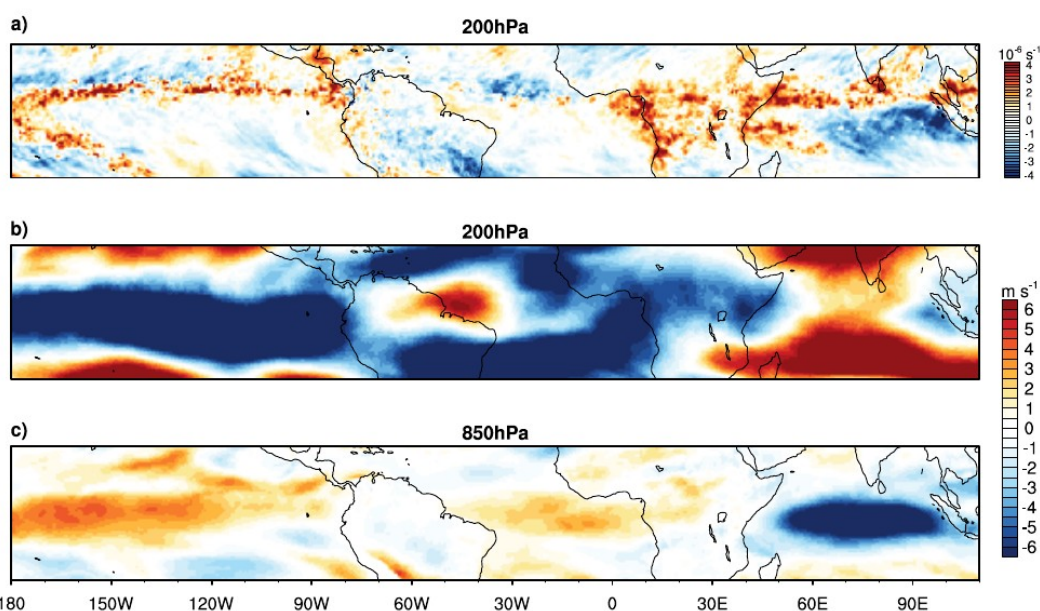
390 From the lower to the high troposphere, anomalous westerly (easterly) winds
391 across the equatorial Atlantic (western Indian) region penetrate the EA domain through its
392 western (eastern) border (Fig. 6a-c). These westerly winds come from the NTA region (at
393 the low troposphere, Fig. 6a).



394 **Fig 6:** Vector wind anomalies (Nov. 2023 minus 1981-2022 mean) at (a) 850 hPa, (b) 650 hPa, (c) 500
395 hPa and (d) 200 hPa.
396
397



398 In addition, over both the equatorial Pacific and Atlantic Oceans, and western EA,
399 westerly anomalies feature at 850 hPa while easterly anomalies are evident over the
400 equatorial Indian Ocean (Fig. 7c). Inverse anomalies are observed at 200 hPa (Fig. 7b),
401 suggesting that the west-east zonal circulation is subject to changes. These later are
402 shown by the upper-level divergence and vertical motion analysis. Equatorial Africa and
403 the coasts of the Atlantic and Indian Oceans feature strong divergence at 200 hPa,
404 followed by strong convergence over the NTA and eastern Indian Ocean regions (Fig. 7a),
405 the reverse divergence anomalies' pattern characterises lower-troposphere level (not
406 shown). These patterns are consistent with Walker circulation, which has been examined
407 by both vertical velocity (ω), and zonal wind combined with vertical velocity (Fig. 8).
408 Note that negative values of ω denote ascent motions and positive values indicate
409 subsidence.
410



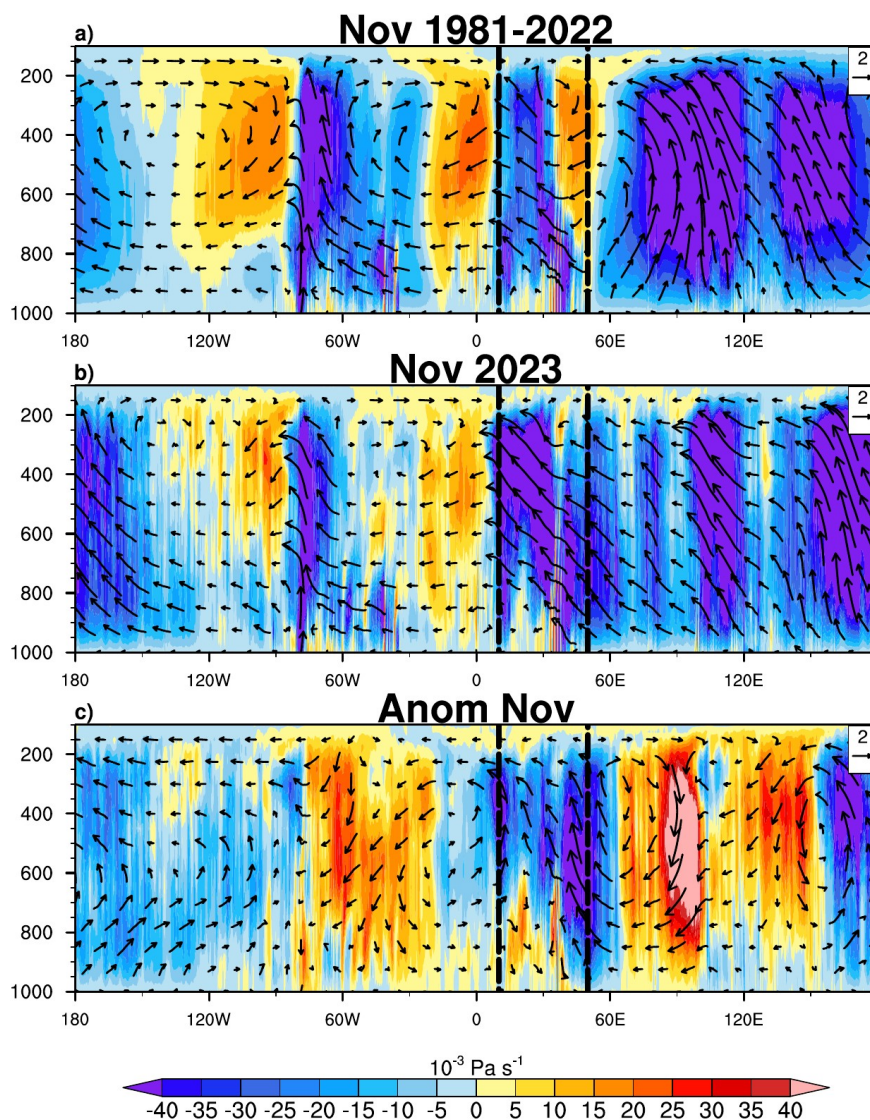
411
412 **Fig 7:** Anomalies of (a) divergence (10^{-6} s^{-1}) at 200 hPa and zonal wind (m s^{-1}) at (b) 200 hPa and (c)
413 850 hPa.
414

415 For the 1981-2022 climatology (Fig. 8a), Omega indicates that the ascent motions
416 of the Indian Ocean Walker cell are very pronounced. The western Atlantic Ocean is
417 characterized by strong rising motions, while the eastern Atlantic Ocean experiences
418 sinking motions. Over western Africa (10° E to 30° E), the entire atmospheric column
419 shows significant upward motion, whereas in eastern Africa (30° E to 45° E), rising
420 motions dominates at low levels, while sinking motions prevails in the mid- and upper
421 troposphere. This subsidence in eastern Africa leads to reduced rainfall. These findings
422 are consistent with those observed during the exceptional October/November 2019



423 events, as noted by [Nicholson et al. \(2022\)](#). By contrast, these branches are weak in
424 general during November 2023 ([Fig. 8b](#)). In contrast to climatology, 2023 shows strong
425 ascendance at mid- and upper-troposphere over eastern Africa. Here, we focus on three
426 omega (color), and zonal wind combined with vertical velocity (vector) patterns to evaluate
427 the location and strength of the African Walker circulation cells. Anomalous rising motion
428 corresponds to areas with low-level converging vectors, mid-level ascent motions and
429 upper-level diverging vectors that will typically experience more rainfall. Following [Fig. 8c](#),
430 at 850 hPa, anomalous rising (sinking) motions are associated with areas of westerly
431 (easterly) anomalies. At 200 hPa, anomalous ascendance (subsidence) corresponds to
432 areas of easterly (westerly) anomalies.

433 It is noteworthy that rainfall deficits are observed over the Congo Basin, around 15-
434 35° E. This region of rainfall deficits is linked to a corresponding area of reduced rising
435 motion at low levels ([Fig. 8c](#)). Over the three oceans, the zonal cells are weaker, but more
436 pronounced over the Atlantic and Indian oceans than the Pacific ocean. In the case of the
437 Pacific Ocean, the increase of Pacific cells is linked with the El Niño events and are moved
438 westward and vertical motion anomalies are weak along the coast of South America. Thus,
439 the SST's El Niño pattern could be highly developed. Both the Atlantic and Indian Oceans
440 feature greater vertical motion contrasts than the Pacific Ocean. This is characterised by
441 an increased ascent (subsidence) over the eastern and western Atlantic and Indian oceans
442 respectively, and increased subsidence (ascent) over the western and eastern Atlantic and
443 Indian oceans respectively. The consequence is a strengthening of the ascent which
444 extends over equatorial Africa and is accompanied by an increase in rainfall over Africa,
445 mainly in East Africa.



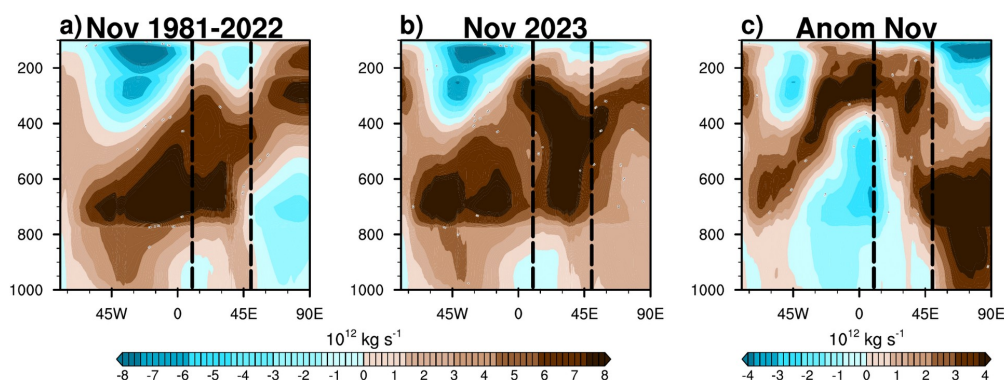
446
447 **Fig 8:** Longitude-height cross-sections of vertical velocity (Ω : 10^{-3} m s^{-1}) selected over latitude
448 10° S - 10° N in November for (top to bottom) climatology, November 2023, and anomaly. The
449 shading (background) represents the vertical velocity, with negative values denoting ascent
450 motions and positive values indicating subsidence. Additionally, the vectors (overlay), obtained with
451 the zonal wind component and vertical velocity, illustrate the behavior of the air mass during
452 upward or downward movements

453

454 To further investigate the vertical motion, the water vapor mass transported
455 analysis is done through the mass-weighted stream-function (Fig. 9). In the climatology
456 mean (Fig. 9a), the CB cell ($\psi < 0$) is located between 1° and 18° E and extends up to 950



457 hPa, whereas it occurs at -1 and 28° E and extends around 975 hPa during November
458 2023 (Fig. 9b). These CB cell locations coincide with the Walker cell ascending branch (Fig.
459 8a,b) over EA, more intense during November 2023 associated with sinking branches over
460 the Equatorial Atlantic and Indian Oceans (Figs. 8c and 9c). Near to 800 hPa, the westward
461 ($\psi > 0$) of the circulation is greater during November 2023 (Fig. 9c), leading to the
462 presence of easterly Jet at the middle-tropospheric. These results confirm those obtained
463 by the Walker circulation and, consequently, the pattern of rainfall anomalies.
464



465
466 **Fig 9:** Zonal mass-weighted stream function (contours: 10^{11} kg s^{-1}) averaged between 10° S- 10° N
467 for (a) mean, (b) Nov. 2023 and (c) Nov. 2023 minus mean. Positive (negative) values indicate the
468 westward (eastward) circulation.

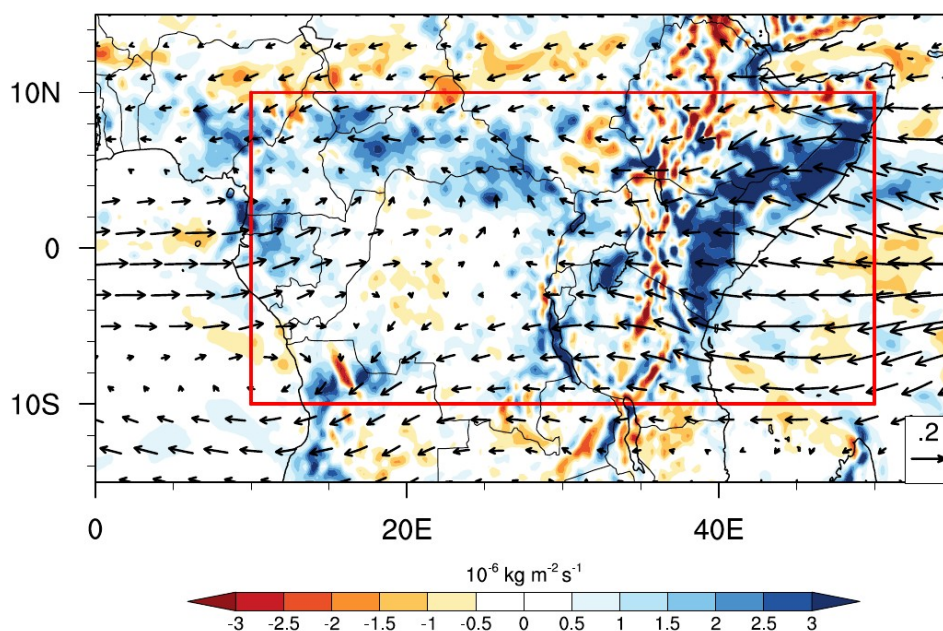
469 4.2.2. Moisture flux divergence

470 **Figure 10** shows the vertically integrated (1000-200 hPa) moisture flux convergence
471 (color) and vertically integrated moisture flux (vectors). Positive values indicated
472 convergence and negative values indicated divergence. Overall, the whole of EA exhibits
473 moisture convergence with strong and significant moisture convergence in areas which
474 feature strong and positive rainfall anomalies (Fig. 1c,f). The weak moisture divergence
475 observed over the central part of DRC confirms the weak and negative rainfall anomalies
476 also observed in this area. Note that all vectors in the EA region originate from the two
477 neighbouring oceans through the western and eastern boundaries only. No vectors have
478 entered the region across the northern and southern boundaries. This confirms that these
479 two oceans were mainly responsible for the wet episodes of 2023. The strong westerly
480 winds become southwesterly to easterly, advecting moist air from the Atlantic Ocean
481 towards the northern regions (Gabon, northern DRC, CAR and Cameroon). It is
482 noteworthy that the strong westerly winds over the equatorial Atlantic originate from the
483 NTA region, where strong and significant moisture divergence has been observed (not
484 shown). For the eastern EA boundary, strong easterly winds from the Indian Ocean advect
485 moist air in eastern and some southern regions, mainly over Somalia, southwest Ethiopia,
486 eastern Kenya, Uganda and northern Angola. These results confirm the warm SST feature
487 over oceans in **Figure 2**. Although the November 2023 DMI is lower than in 2019 when the
488 strongest positive IOD event since the 1950s occurred during October and November



489 (Nicholson et al. 2022), the eastern region of EA was wetter in 2023 compared to 2019.
490 This can be seen through the convergence and moisture flux anomalies, and
491 consequently the higher precipitation in November 2023. One explanation could be the
492 significant presence of the El Niño event in 2023, which contributed to humidifying the
493 Eastern Africa region (Palmer et al. 2023; Roy and Troccoli 2024), unlike 2019, when during
494 the positive IOD event, the El Niño episode was absent (Nicholson et al. 2022).

495



496
497 **Fig 10:** (a) Anomalies of vertically integrated (1000-200 hPa) moisture flux (vectors: $\text{kg m}^{-1} \text{s}^{-1}$) and
498 vertically integrated moisture flux convergence (positive values) or divergence (negative values)
499 anomalies (shading: $10^{-6} \text{ kg m}^{-2} \text{ s}^{-1}$). Only significant vectors (shading) above the 90 % (95 %) level
500 are shown

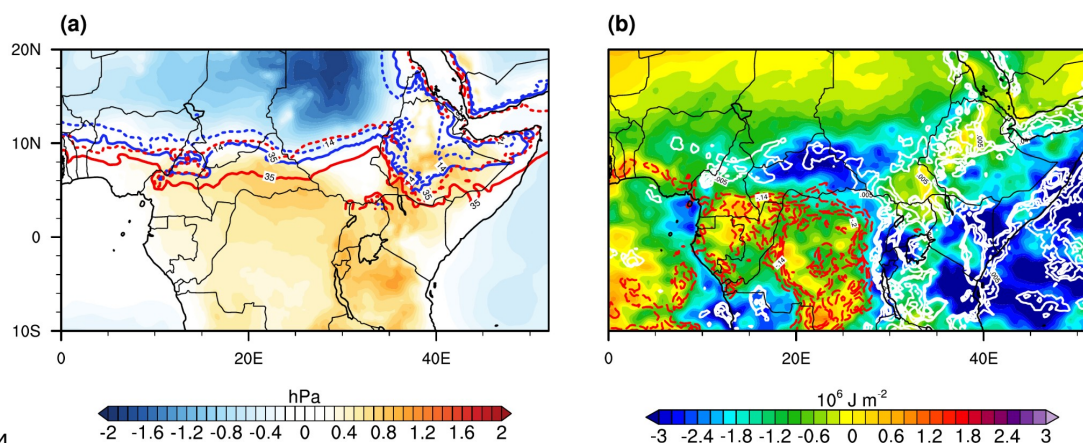
501

502 The northern regions (western Nigeria, northern Cameroon, southern Chad, CAR
503 and South Sudan), which receive less than 2 mm day^{-1} of rainfall and have a near zero
504 percentage contribution of November rainfall (Fig. 1a-b, d-e), recorded heavy rainfall in
505 November 2023 (Fig. 1c-f). Similar to Nicholson et al. (2022) in October 2019, Figure 11a
506 confirms this northward displacement of the state of the African monsoon in November
507 2023. During this year, the 35 mm isopleth of the total column water vapor and the
508 intertropical discontinuity (dashed blue and red lines respectively) move to the north,
509 enhancing rainfall in the northern regions. These dashed lines correspond to the limit of
510 the anomalous meridional mean sea level pressure gradient, characterised by anomalous
511 high pressure over the south of the 35 mm isopleth of the total column water vapor and
512 the intertropical discontinuity lines, and lower over the north. Except over the Eastern EA



513 areas. Similar pressure, intertropical discontinuity and 35 mm isopleth of the total column
514 water vapor, and easterly (westerly) moisture flux anomaly were observed over Eastern EA
515 (Gabon, CAR and Chad) in October (November) 2019 when extreme rainfall and flooding
516 occurred in the latter country (Nicholson et al. 2022). As shown in Figure 11b, low-cloud
517 cover (LCC) is below average in the southwest of EA (mainly over CB and south of
518 Cameroon and Gabon) but becomes above average over the northern part of EA (mainly
519 over CAR) and the whole of East Africa. These positive LCC anomalies coincide with
520 positive and strong surface net solar radiation anomalies. These spatial differences in
521 atmospheric convective activity revealed by LCC and surface net solar radiation explain
522 the spatial variations in rainfall anomalies shown in Fig. 1c,f.

523



524

525 **Fig 11:** (a) The anomalous state of the African monsoon in November 2023 is characterized by
526 mean sea-level pressure anomalies (colored) relative to the 1981-2022 average, along with the
527 positions of the intertropical discontinuity (ITD) and total column water vapor isopleths. The ITD is
528 indicated by the 14°C 2-meter dew point temperature contours, with the mean ITD position shown
529 by a solid blue line and the November 2023 position by a dashed blue line. Similarly, the mean
530 location of the 35 mm total column water vapor isopleths is marked by a solid red line, while the
531 November 2023 position is represented by a dashed red line. (b) Spatial representation of the
532 surface net solar radiation anomalies (shading: 10⁶ J m⁻²). Red (white) lines represent negative
533 (positive) low cloud cover (%) anomalies.

534 4.2.3. LLWs, easterly Jets and MJO activity

535

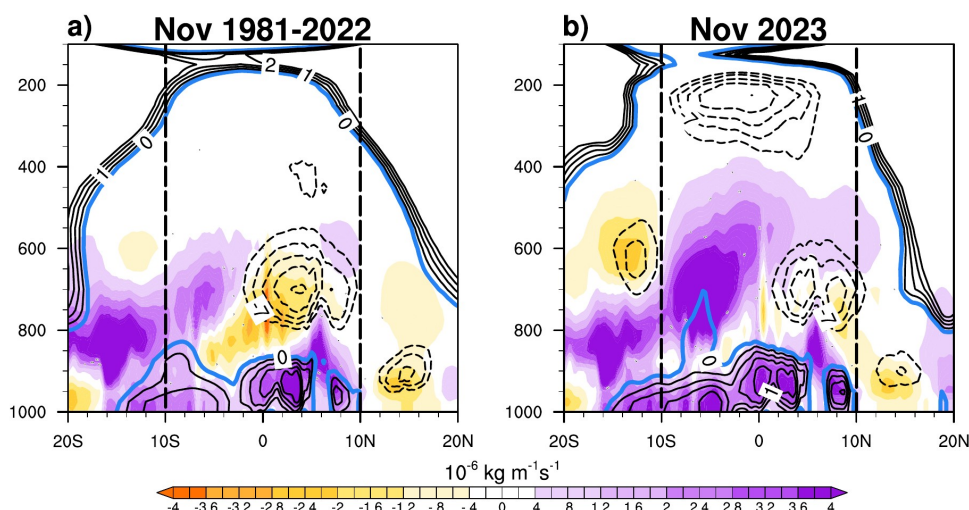
536 One of the key atmospheric features over western EA are the African Easterly Jet
537 (AEJ) and Tropical Easterly Jet (TEJ). Following Nicholson and Grist (2003), AEJ and TEJ are
538 maximum easterly winds that occur at the mid-troposphere (from 700 to 600 hPa) and
539 upper-troposphere (around 200 hPa) respectively. Here, we describe the characteristics of
540 these atmospheric features during the Nov 2023 extreme rainfall. The African Easterly Jet's
541 southern component (AEJ-S) only appears from September to November and its jet core is



542 located around 10° S in November (Kuete et al. 2022). In contrast to the AEJ-S, the
543 northern component (AEJ-N) occurs during all months of the year, and its core is located
544 around 5° N in November. As the AEJ-N, TEJ features during all months and is located near
545 the south equator. Nicholson and Grist (2003) showed that Central Africa is a region
546 where the divergence of the upper troposphere (Fig. 7a) is enhanced, which could favour
547 convective activity (Fig. 8c), suggesting that the variability of the TEJ may influence the
548 variability of precipitation in the region. Figure 12 shows Latitude/height cross-sections of
549 easterly winds (dashed contours) of the 1981-2022 November mean and November 2023
550 at 10° E, overlaid by the zonal moisture flux (color) calculated from the West boundary
551 (10° E) minus East boundary (30° E).

552 For the mean climatology (Fig. 12a), only AEJ-N is observed around 3° N at 700 hPa,
553 with core speeds reaching 10 m s^{-1} . This intensification of AEJ-N coincides with strong
554 moisture flux divergence. During November 2023 (Fig. 12b), both AEJ components and TEJ
555 are present at the mid- and upper-troposphere respectively. During this year, the mid-
556 level zonal moisture convergence (divergence) induced by the weak AEJ-S (jet core not
557 exceeding 7 m s^{-1} ; Kuete et al., 2019) increases (decreases), favoring increases mid-
558 tropospheric moisture convergence south of the equator over western EA, resulting in
559 wet conditions over the domain (Fig. 1c,f). AEJ-N moves further north and its intensity
560 decreases from 10 m s^{-1} to 8 m s^{-1} , leading also to more western EA rainfall during positive
561 IOD events, more pronounced during the October-November months (Moihamette et al.
562 2024). Following Moihamette et al. (2024), this decrease of the AEJ-N drove the equatorial
563 easterly moisture transport to the western EA. These conclusions are in agreement with a
564 study by Dezfuli and Nicholson (2013) showing that during October and November, the
565 months with stronger (weaker) AEJ components experience dry (wet) conditions over
566 western EA. Also, Nicholson and Grist (2003) showed that when both AEJ components are
567 present, the western EA's rain-band moves further south (10° S to the equator), this is only
568 observed during November. Another feature is the LLWs, which are weak in climatology,
569 were anomalously strong and extended up to 700 hPa, mainly over southern-hemisphere
570 latitudes. These wind changes lead to enhanced rainfall in western EA during the SON
571 seasons (Pokam et al. 2014; Kuete et al. 2019; Taguela et al. 2022).

572



573

574

575

576

577

578

579

580

581

582

583

584

585

586

587

588

589

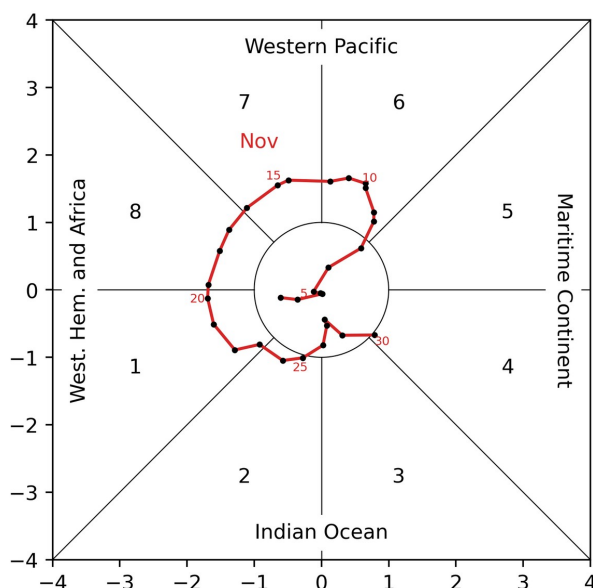
590

591

592

Fig 12: Latitude/height cross-sections of net zonal moisture flux ($10^{-6} \text{ kg m}^{-1} \text{ s}^{-1}$) calculated from West boundary (10° E) minus East boundary (30° E) for (a) climatology and (b) November 2023. Black solid (dashed) lines represent LLW (AEJ) components and TEJ; $U < -6 \text{ m s}^{-1}$ with the contour interval of 0.5 (1) m s^{-1} , calculated at 10° E for the respective periods. Positive values indicate moisture flux convergence, and negative values moisture flux divergence.

Here, we analyse one of eastern Africa's intra-seasonal climate drivers, the MJO, through the Real-time Multivariate MJO (RMM) index. This later strongly influences the equatorial Africa region's rainfall during March-April-May (Sandjon et al. 2012) and November and December (Pohl and Camberlin 2006; Berhane and Zaitchik 2014; Berhane 2016; Zaitchik 2017; Palmer et al. 2023). According to Pohl and Camberlin (2006) and Kimani et al. (2020), during phases 6-8 (1-4) of the MJO, there is an increased chance of the highest rainfall over the coastal (highlands) regions of East Africa during OND months, through moisture advection from the Indian Ocean. The ENSO-MJO relationship was studied by Pohl and Matthews (2007), who found that maximum MJO activity is often observed during El-Niño events. In addition, Berhane (2016) showed that this juxtaposition of MJO activity and ENSO events leads to an increase in precipitation that is greater than when El-Niño events are absent.



593
594 **Fig 13:** Madden-Julian Oscillation (MJO) phases and intensity (red line) space diagram for November
595 2023. Each black dot represents the value for a given day with select dates labelled in red. [Source:
596 NOAA/NCEI Climate.gov, [https://www.ncei.noaa.gov/access/monitoring/monthly-report/synoptic/
597 202311](https://www.ncei.noaa.gov/access/monitoring/monthly-report/synoptic/202311), accessed 26/11/24]

598
599 **Figure 13** shows the MJO phase space diagram for November 2023, based on the
600 RMM index. It should be noted that the MJO was active for 19 days, during phases leading
601 to wet periods in the highlands and coastal areas of East Africa (Pohl and Camberlin 2006;
602 Berhane and Zaitchik 2014; Zaitchik 2017). During November 2023, the MJO was in phases
603 6-8 from 8 to 19 November, which are the phases leading to wet spells over the East
604 African coast (Pohl and Camberlin 2006; Zaitchik 2017), mainly over Somalia and the
605 eastern parts of Ethiopia, Tanzania and Kenya regions. Also, during 20-25 and 30
606 November 2023, the MJO was in phases 1, 2 and 4, which are the phases typically
607 associated with increased rainfall over the Highland region of East Africa (Pohl and
608 Camberlin 2006), mainly over Uganda, the western and northern part of Kenya and
609 Tanzania, respectively.

610 **5. Summary and Conclusions**

611

612 This study examines the extreme wet conditions that occurred in November 2023
613 in Equatorial Africa (EA) and shows that this rainy episode was caused by several factors.
614 While some anomalous rainfall over both western and eastern equatorial Africa were
615 attributed to moisture transport from the Atlantic and Indian oceans respectively, the
616 unusually very strong November 2023 MJO activity was a significant factor. In addition to
617 meteorological conditions, further research is therefore needed to quantify the roles that



618 dynamic and thermodynamic processes played in the extreme events of November 2023.

619 The most important findings of this study are as follows:

- 620 - Although the rain band in November is over the south equator, many north
621 areas feature positive rainfall anomalies, most pronounced over eastern
622 Africa. These strongest November 2023 rainfall anomalies occur when
623 significant SST anomalies were observed in the three equatorial oceans.
- 624 - In contrast to the extreme rainfall of November 2019 in East Africa, where
625 the DMI reached record levels, the DMI of November 2023, which is lower
626 than that of 2019, is causing more rainfall. This may be due to the presence
627 of strong El Nino conditions over the equatorial Pacific in 2023. But over
628 central Africa, the rainfall anomalies in 2023 are lower than in 2019,
629 certainly due to the state of the equatorial Atlantic Ocean, which was
630 warmer in 2019 than in 2023.
- 631 - SST anomalies over the Atlantic (Indian) Ocean are associated with
632 anomalous westerly (easterly) winds that bring more moisture over EA ([Fig.](#)
633 [5c](#)). Moisture flux from both oceans, respectively ([Fig. 5f](#)), induced a
634 weakening of the ascending and descending branches of both neighboring
635 oceans Walker-like cells ([Figs. 8 and 9](#)).
- 636 - The westerly moisture flux from the Atlantic Ocean that veered into
637 southwesterlies moved the rainbelt further north by enhancing the
638 transport of moist air over the northern (5°-10° N) regions ([Fig. 11](#)).
- 639 - Over western EA where extreme rain also occurs, the African wind and
640 easterly wind regime is an important factor. The presence of strong
641 equatorial westerlies, AEJ-S and TEJ, and the movement of AEJ-N further
642 north have also retarded the retreat of the West African monsoon, causing
643 positive rainfall anomalies over northern areas (especially over Nigeria,
644 Cameroon, CAR, Sudan and South Chad).
- 645 - Another driver is the MJO activity, which was active during several days of
646 November 2023 ([Fig. 12](#)). We have shown that the positive rainfall anomalies
647 over East Africa coincided with active phases of MJO, which enhanced
648 rainfall in November over both western and eastern areas of East Africa.
649 This increase in rainfall was significant with the occurrence of the El-Niño
650 events.

651 This study demonstrates that the anomalous wetness conditions over Equatorial
652 Africa were caused mainly by the Atlantic and Indian oceans, through the anomalous
653 moisture transport and moisture flux divergence, Walker circulation, and changes in the
654 zonal winds, induced by extremely strong SST anomalies. These anomalous patterns were
655 similar to those observed over this region in October/November 2019 when extreme
656 rainfall occurred, following [Nicholson et al. \(2021\)](#). The present study demonstrates the
657 importance of accounting for ocean-atmosphere interactions in intra-seasonal forecast



658 models to refine regional climate information provided to policymakers. It is important to
659 highlight that the robustness of these findings requires additional evaluation. Our study
660 exclusively examines the meteorological causes of these extreme events. Further
661 investigations should encompass the roles that dynamic and thermodynamic processes
662 played in these November 2023 events.

663

664

665

666

667

668

669

670

671

672

673

674

675

676

677

678

679

680

681

682

683

684

685

686

687

688

689

690

691

692

693

694

695

696



697 **Code availability** Figures shown in this study are plotted using the NCAR Command
698 Language (NCL; <https://doi.org/10.5065/D6WD3XH5>, NCAR Command Language, 2017).
699 Codes can be obtained from the corresponding author.

700

701 **Data Availability Statement** All observational and reanalysis data used in this study are
702 publicly available at no charge and with unrestricted access. One plot is generated using
703 the web site of NOAA/NCEI, at <https://www.ncei.noaa.gov/>. The ERA5 reanalysis is
704 produced within the Copernicus Climate Change Service (C3S) by the ECMWF and is
705 accessible via the link [https://cds.climate.copernicus.eu/datasets/reanalysis-era5-](https://cds.climate.copernicus.eu/datasets/reanalysis-era5-pressure-levels-monthly-means?tab=download)
706 [pressure-levels-monthly-means?tab=download](https://cds.climate.copernicus.eu/datasets/reanalysis-era5-pressure-levels-monthly-means?tab=download); the CHIRPS2 data are available at
707 https://data.chc.ucsb.edu/products/CHIRPS-2.0/global_daily/netcdf/; the ERSST data are
708 available at <https://iridl.ldeo.columbia.edu/SOURCES/.NOAA/.NCDC/.ERSST/.version5/>.

709

710 **Author's contributions**

711 **HNN:** Conceptualization; data upload; data analysis; formal analysis; investigation;
712 methodology; software; validation; writing-original draft; writing-review and editing. **MG:**
713 Project administration; supervision; formal analysis; investigation; validation; writing-
714 original draft; writing-review and editing. **RST:** Project administration; supervision;
715 validation; methodology; writing; review and editing. **ATT:** Project administration;
716 validation; methodology; writing; review and editing. **DAV:** Project administration;
717 supervision; validation, methodology; writing; review and editing.

718

719 **Conflict of Interest** The authors declare no conflicts of interest relevant to this study.

720

721 **Funding** Not applicable

722

723 **Acknowledgements** The authors thank you to all reanalysis, observational and satellite
724 data providers used in this study. We would like to express our gratitude to the
725 anonymous reviewers, along with the editor for their constructive suggestions, which
726 have greatly improved the quality of the paper. We gratefully appreciate the efforts of the
727 International Joint Laboratory Dynamics of Terrestrial Ecosystems in Central Africa (IJL
728 DYCOCA/ LMI DYCOFAC) initiative during the realisation of this work.

729

730

731

732

733

734

735



736 **References**

- 737 Berhane, F., & Zaitchik, B. (2014). Modulation of daily precipitation over East Africa by the
738 madden-julian oscillation*. *Journal of Climate*, 27(15), 6016–6034.
739 <https://doi.org/10.1175/jcli-d-13-00693.1>
- 740 Berhane, F., 2016. Intraseasonal Precipitation Variability Over Tropical Africa. PhD, Johns
741 Hopkins University, Baltimore, MD, USA,
- 742 Chadwick, R., Good, P., & Willett, K. (2016). A simple moisture advection model of specific
743 humidity change over land in response to SST warming. *Journal of Climate*, 29(21),
744 7613–7632. <https://doi.org/10.1175/jcli-d-16-0241.1>
- 745 Chobo, J. S., & Huo, L. (2024). The relationship between extreme precipitation events in
746 East Africa during the short rainy season and Indian Ocean Sea surface
747 temperature. *Journal of Geoscience and Environment Protection*, 12(09), 1–16.
748 <https://doi.org/10.4236/gep.2024.129001>
- 749 Dezfuli, A. K., & Nicholson, S. E. (2013). The relationship of rainfall variability in Western
750 Equatorial Africa to the tropical oceans and atmospheric circulation. Part II: The
751 Boreal Autumn. *Journal of Climate*, 26(1), 66–84. <https://doi.org/10.1175/jcli-d-11-00686.1>
- 752
- 753 Fotso-Nguemo, T. C., Diallo, I., Diakhaté, M., Vondou, D. A., Mbaye, M. L., Haensler, A.,
754 Gaye, A. T., & Tchawoua, C. (2019). Projected changes in the seasonal cycle of
755 extreme rainfall events from CORDEX simulations over Central Africa. *Climatic
756 Change*, 155(3), 339–357. <https://doi.org/10.1007/s10584-019-02492-9>
- 757 Funk, C., Dettinger, M. D., Michaelsen, J. C., Verdin, J. P., Brown, M. E., Barlow, M., & Hoell,
758 A. (2008). Warming of the Indian Ocean threatens eastern and southern African
759 food security but could be mitigated by agricultural development. *Proceedings of
760 the National Academy of Sciences*, 105(32), 11081–11086.
761 <https://doi.org/10.1073/pnas.0708196105>
- 762 Gudoshava, M., Misiani, H. O., Segele, Z. T., Jain, S., Ouma, J. O., Otieno, G., Anyah, R.,
763 Indasi, V. S., Endris, H. S., Osima, S., Lennard, C., Zaroug, M., Mwangi, E.,
764 Nimusiima, A., Kondowe, A., Ogwang, B., Artan, G., & Atheru, Z. (2020). Projected
765 effects of 1.5 °C and 2 °C global warming levels on the intra-seasonal rainfall
766 characteristics over the Greater Horn of Africa. *Environmental Research Letters*, 15(3),
767 034037. <https://doi.org/10.1088/1748-9326/ab6b33>
- 768 Gudoshava, M., Nyinguro, P., Talib, J., Wainwright, C., Mwanthi, A., Hirons, L., de Andrade,
769 F., Mutemi, J., Gitau, W., Thompson, E., Gacheru, J., Marsham, J., Endris, H. S.,
770 Woolnough, S., Segele, Z., Atheru, Z., & Artan, G. (2024). Drivers of sub-seasonal
771 extreme rainfall and their representation in ECMWF forecasts during the Eastern
772 African March-to-May seasons of 2018–2020. *Meteorological Applications*, 31(5).
773 <https://doi.org/10.1002/met.70000>
- 774 Indeje, M., Semazzi, F. H. M., & Ogallo, L. J. (2000). ENSO signals in East African rainfall
775 seasons. *International Journal of Climatology*, 20(1), 19–46.



- 776 [https://doi.org/10.1002/\(sici\)1097-0088\(200001\)20:1<19::aid-joc449>3.0.co;2-0](https://doi.org/10.1002/(sici)1097-0088(200001)20:1<19::aid-joc449>3.0.co;2-0)
777 Ingeri, C., Wen, W., Sebaziga, J. N., Iyakaremye, V., Ekwacu, S., Ayabagabo, P., Twahirwa,
778 A., & Kazora, J. (2024). Potential driving systems associated with extreme rainfall
779 across East Africa during october to december (OND) season 2019. *Journal of*
780 *Geoscience and Environment Protection*, 12(07), 25–49.
781 <https://doi.org/10.4236/gep.2024.127003>
782 Kenfack, K., Marra, F., Djomou, Z. Y., Tchotchou, L. A. D., Tamoffo, A. T., & Vondou, D. A.
783 (2024). Dynamic and thermodynamic contribution to the October 2019 exceptional
784 rainfall in western central Africa. *Weather and Climate Dynamics*, 5(4), 1457–1472.
785 <https://doi.org/10.5194/wcd-5-1457-2024>
786 Kilavi, M., MacLeod, D., Ambani, M., Robbins, J., Dankers, R., Graham, R., Titley, H., Salih, A.,
787 & Todd, M. (2018). Extreme rainfall and flooding over central kenya including
788 nairobi city during the long-rains season 2018: Causes, predictability, and potential
789 for early warning and actions. *Atmosphere*, 9(12), 472.
790 <https://doi.org/10.3390/atmos9120472>
791 Kimani, M., Hoedjes, J. C. B., & Su, Z. (2020). An assessment of MJO circulation influence on
792 air–sea interactions for improved seasonal rainfall predictions over East Africa.
793 *Journal of Climate*, 33(19), 8367–8379. <https://doi.org/10.1175/jcli-d-19-0296.1>
794 Kuete, G., Mba, W. P., James, R., Dyer, E., Annor, T., & Washington, R. (2022). How do
795 coupled models represent the African Easterly Jets and their associated dynamics
796 over Central Africa during the September–November rainy season? *Climate*
797 *Dynamics*, 60(9–10), 2907–2929. <https://doi.org/10.1007/s00382-022-06467-y>
798 Kuete, G., Pokam Mba, W., & Washington, R. (2019). African Easterly Jet South: Control,
799 maintenance mechanisms and link with Southern subtropical waves. *Climate*
800 *Dynamics*, 54(3–4), 1539–1552. <https://doi.org/10.1007/s00382-019-05072-w>
801 Li, C., Chai, Y., Yang, L., & Li, H. (2016). Spatio-temporal distribution of flood disasters and
802 analysis of influencing factors in Africa. *Natural Hazards*, 82(1), 721–731.
803 <https://doi.org/10.1007/s11069-016-2181-8>
804 Longandjo, G.-N. T., & Rouault, M. (2020). On the structure of the regional-scale circulation
805 over Central Africa: Seasonal evolution, variability, and mechanisms. *Journal of*
806 *Climate*, 33(1), 145–162. <https://doi.org/10.1175/jcli-d-19-0176.1>
807 Longandjo, G.-N. T., & Rouault, M. (2024). Revisiting the seasonal cycle of rainfall over
808 Central Africa. *Journal of Climate*, 37(3), 1015–1032. [https://doi.org/10.1175/jcli-d-23-](https://doi.org/10.1175/jcli-d-23-0281.1)
809 [0281.1](https://doi.org/10.1175/jcli-d-23-0281.1)
810 Lüdecke, H.-J., Müller-Plath, G., Wallace, M. G., & Lüning, S. (2021). Decadal and
811 multidecadal natural variability of African rainfall. *Journal of Hydrology: Regional*
812 *Studies*, 34, 100795. <https://doi.org/10.1016/j.ejrh.2021.100795>
813 Lutz, K., Jacobeit, J., & Rathmann, J. (2014). Atlantic warm and cold water events and
814 impact on African west coast precipitation. *International Journal of Climatology*,
815 35(1), 128–141. <https://doi.org/10.1002/joc.3969>



- 816 Madden, R. A., & Julian, P. R. (1971). Detection of a 40–50 day oscillation in the zonal wind
817 in the Tropical Pacific. *Journal of the Atmospheric Sciences*, 28(5), 702–708.
818 [https://doi.org/10.1175/1520-0469\(1971\)028<0702:doadoi>2.0.co;2](https://doi.org/10.1175/1520-0469(1971)028<0702:doadoi>2.0.co;2)
- 819 Madden, R. A., & Julian, P. R. (1972). Description of global-scale circulation cells in the
820 Tropics with a 40–50 day period. *Journal of the Atmospheric Sciences*, 29(6), 1109–
821 1123. [https://doi.org/10.1175/1520-0469\(1972\)029<1109:dogsc>2.0.co;2](https://doi.org/10.1175/1520-0469(1972)029<1109:dogsc>2.0.co;2)
- 822 McHugh, M. J., & Rogers, J. C. (2001). North atlantic oscillation influence on precipitation
823 variability around the southeast african convergence zone. *Journal of Climate*,
824 14(17), 3631–3642. [https://doi.org/10.1175/1520-0442\(2001\)014<3631:naoiop>2.0.co;2](https://doi.org/10.1175/1520-0442(2001)014<3631:naoiop>2.0.co;2)
- 826 Moihamette, F., Pokam, W. M., Diallo, I., & Washington, R. (2022). Extreme Indian Ocean
827 dipole and rainfall variability over Central Africa. *International Journal of Climatology*,
828 42(10), 5255–5272. <https://doi.org/10.1002/joc.7531>
- 829 Moihamette, F., Pokam, W. M., Diallo, I., & Washington, R. (2024). Response of regional
830 circulation features to the Indian Ocean dipole and influence on Central Africa
831 climate. *Climate Dynamics*, 62(6), 1–21. <https://doi.org/10.1007/s00382-024-07251-w>
- 832 Nana, H. N., Tamoffo, A. T., Kaissassou, S., Djiotang Tchotchou, L. A., Tanessong, R. S.,
833 Kamsu-Tamo, P. H., Kenfack, K., & Vondou, D. A. (2024). Performance-based
834 evaluation of NMME and C3S models in forecasting the June–August Central
835 African rainfall under the influence of the South Atlantic Ocean Dipole.
836 *International Journal of Climatology*, 44(7), 2462–2483.
837 <https://doi.org/10.1002/joc.8463>
- 838 Nana, H. N., Tanessong, R. S., Tchotchou, L. A. D., Tamoffo, A. T., Moihamette, F., &
839 Vondou, D. A. (2023). Influence of strong South Atlantic Ocean Dipole on the
840 Central African rainfall's system. *Climate Dynamics*, 62(1), 1–16.
841 <https://doi.org/10.1007/s00382-023-06892-7>
- 842 Ngavom, Z., Fotso-Nguemo, T. C., Vondou, D. A., Fotso-Kamga, G., Zebaze, S., Yepdo, Z. D.,
843 & Diedhiou, A. (2024). Projected changes in population exposure to extreme
844 precipitation events over Central Africa under the global warming levels of 1.5 °C
845 and 2 °C: Insights from CMIP6 simulations. *Modeling Earth Systems and Environment*,
846 10(4), 5753–5769. <https://doi.org/10.1007/s40808-024-02091-3>
- 847 Nicholson, S. E. (2015). Long-term variability of the East African ‘short rains’ and its links to
848 large-scale factors. *International Journal of Climatology*, 35(13), 3979–3990.
849 <https://doi.org/10.1002/joc.4259>
- 850 Nicholson, S. E., Fink, A. H., Funk, C., Klotter, D. A., & Satheesh, A. R. (2022). Meteorological
851 causes of the catastrophic rains of October/November 2019 in equatorial Africa.
852 *Global and Planetary Change*, 208, 103687.
853 <https://doi.org/10.1016/j.gloplacha.2021.103687>
- 854 Nicholson, S. E., & Grist, J. P. (2003). The seasonal evolution of the atmospheric circulation
855 over West Africa and Equatorial Africa. *Journal of Climate*, 16(7), 1013–1030.



- 856 [https://doi.org/10.1175/1520-0442\(2003\)016<1013:tseota>2.0.co;2](https://doi.org/10.1175/1520-0442(2003)016<1013:tseota>2.0.co;2)
857 Onyutha, C. (2016). Geospatial trends and decadal anomalies in extreme rainfall over
858 uganda, east africa. *Advances in Meteorology*, 2016, 1–15.
859 <https://doi.org/10.1155/2016/6935912>
860 Palmer, P. I., Wainwright, C. M., Dong, B., Maidment, R. I., Wheeler, K. G., Gedney, N.,
861 Hickman, J. E., Madani, N., Folwell, S. S., Abdo, G., Allan, R. P., Black, E. C. L., Feng, L.,
862 Gudoshava, M., Haines, K., Huntingford, C., Kilavi, M., Lunt, M. F., Shaaban, A., &
863 Turner, A. G. (2023). Drivers and impacts of Eastern African rainfall variability.
864 *Nature Reviews Earth & Environment*, 4(4), 254–270.
865 <https://doi.org/10.1038/s43017-023-00397-x>
866 Pohl, B., & Camberlin, P. (2006). Influence of the Madden–Julian Oscillation on East African
867 rainfall. I: Intraseasonal variability and regional dependency. *Quarterly Journal of*
868 *the Royal Meteorological Society*, 132(621), 2521–2539.
869 <https://doi.org/10.1256/qj.05.104>
870 Pohl, B., & Matthews, A. J. (2007). Observed changes in the lifetime and amplitude of the
871 madden–julian oscillation associated with interannual ENSO sea surface
872 temperature anomalies. *Journal of Climate*, 20(11), 2659–2674.
873 <https://doi.org/10.1175/jcli4230.1>
874 Pokam, W. M., Bain, C. L., Chadwick, R. S., Graham, R., Sonwa, D. J., & Kamga, F. M. (2014).
875 Identification of processes driving low-level westerlies in west equatorial africa.
876 *Journal of Climate*, 27(11), 4245–4262. <https://doi.org/10.1175/jcli-d-13-00490.1>
877 Pokam, W. M., Djiotang, L. A. T., & Mkankam, F. K. (2011). Atmospheric water vapor
878 transport and recycling in Equatorial Central Africa through NCEP/NCAR reanalysis
879 data. *Climate Dynamics*, 38(9–10), 1715–1729. [https://doi.org/10.1007/s00382-011-](https://doi.org/10.1007/s00382-011-1242-7)
880 [1242-7](https://doi.org/10.1007/s00382-011-1242-7)
881 Roy, I., & Troccoli, A. (2024). Identifying important drivers of East African October to
882 December rainfall season. *Science of The Total Environment*, 914, 169615.
883 <https://doi.org/10.1016/j.scitotenv.2023.169615>
884 Sandjon, A. T., Nzeukou, A., & Tchawoua, C. (2012). Intraseasonal atmospheric variability
885 and its interannual modulation in Central Africa. *Meteorology and Atmospheric*
886 *Physics*, 117(3–4), 167–179. <https://doi.org/10.1007/s00703-012-0196-6>
887 Seager, R., Naik, N., & Vecchi, G. A. (2010). Thermodynamic and dynamic mechanisms for
888 large-scale changes in the hydrological cycle in response to global warming*.
889 *Journal of Climate*, 23(17), 4651–4668. <https://doi.org/10.1175/2010jcli3655.1>
890 Stachnik, J. P., & Schumacher, C. (2011). A comparison of the Hadley circulation in modern
891 reanalyses. *Journal of Geophysical Research: Atmospheres*, 116(D22), n/a–n/a.
892 <https://doi.org/10.1029/2011jd016677>
893 Taguela, T. N., Pokam, W. M., Dyer, E., James, R., & Washington, R. (2022). Low-level
894 circulation over Central Equatorial Africa as simulated from CMIP5 to CMIP6
895 models. *Climate Dynamics*, 62(9), 8333–8351. <https://doi.org/10.1007/s00382-022->



- 896 06411-0
897 Tamoffo, A. T., Amekudzi, L. K., Weber, T., Vondou, D. A., Yamba, E. I., & Jacob, D. (2022).
898 Mechanisms of rainfall biases in two CORDEX-CORE regional climate models at
899 rainfall peaks over central equatorial africa. *Journal of Climate*, 35(2), 639–668.
900 <https://doi.org/10.1175/jcli-d-21-0487.1>
901 Tamoffo, A. T., Weber, T., Abel, D., Ziegler, K., Cabos, W., Sein, D. V., & Laux, P. (2024).
902 Regionally coupled climate model ROM projects more plausible precipitation
903 change over Central Equatorial Africa. *Journal of Geophysical Research: Atmospheres*,
904 129(21). <https://doi.org/10.1029/2024jd041466>
905 Tanessong, R. S., Vondou, D. A., Djomou, Z. Y., & Igri, P. M. (2017). WRF high resolution
906 simulation of an extreme rainfall event over Douala (Cameroon): A case study.
907 *Modeling Earth Systems and Environment*, 3(3), 927–942.
908 <https://doi.org/10.1007/s40808-017-0343-7>
909 Wahiduzzaman, M., & Luo, J.-J. (2020). A statistical analysis on the contribution of El Niño–
910 Southern Oscillation to the rainfall and temperature over Bangladesh. *Meteorology
911 and Atmospheric Physics*, 133(1), 55–68. <https://doi.org/10.1007/s00703-020-00733-6>
912 Wainwright, C. M., Finney, D. L., Kilavi, M., Black, E., & Marsham, J. H. (2020). Extreme
913 rainfall in East Africa, October 2019–January 2020 and context under future climate
914 change. *Weather*, 76(1), 26–31. <https://doi.org/10.1002/wea.3824>
915 Yao, L., Lu, J., Xia, X., Jing, W., & Liu, Y. (2021). Evaluation of the ERA5 sea surface
916 temperature around the Pacific and the Atlantic. *IEEE Access*, 9, 12067–12073.
917 <https://doi.org/10.1109/access.2021.3051642>
918 Zaitchik, B. F. (2017). Madden-Julian Oscillation impacts on tropical African precipitation.
919 *Atmospheric Research*, 184, 88–102. <https://doi.org/10.1016/j.atmosres.2016.10.002>
920 Zheng, X., & Eltahir, E. A. B. (1998). A Soil Moisture–Rainfall Feedback Mechanism: 2.
921 Numerical experiments. *Water Resources Research*, 34(4), 777–785.
922 <https://doi.org/10.1029/97wr03497>